MATERIALS FORUM VOLUME 31 - 2007
Edited by J.M. Cairney and S.P. Ringer

STRUCTURE-PROPERTY RELATIONS OF METALLIC MATERIALS WITH MULTISCALE MICROSTRUCTURES

C. Yang, I. Sabirov, J. Mullins, N. Yazdipour, S.A. Asgari and P.D. Hodgson

Centre for Material and Fibre Innovation, Geelong Technology Precinct,
Deakin University, Waurn Ponds, Victoria, 3217

ABSTRACT

Nanostructured metals have higher strength than those of the coarse grained metals but suffer from the extremely limited ductility. Development of the multiscale microstructures can improve the ductility of these high strength materials due to the introduction of a specific range of grain sizes in micro level. The present work relates the multiscale microstructures in metals to their overall structure properties using a fractal theory and the modified mean-field method, where three microstructural parameters are introduced and thus mechanical properties such as strength and ductility are presented as a function of these microstructural parameters. Meanwhile, with the applications of the finite element method, the multiscale unit cell approach is also critically developed and applied with a focus on predicting the related stress-strain relations of the metals with multiscale microstructures. For verification of these proposed theoretical and numerical algorithms, the mechanical properties of the pure copper with three-grain microstructures are investigated and the results from FEA and theoretical solutions have a reasonable agreement.

1. INTRODUCTION

Nanostructured metals have attracted growing interests in materials science due to their improved mechanical properties [1]. For instance, pure nanostructured copper has a yield strength of 400 MPa, which is six times higher than that of coarse-grained copper. However, the industrial application of nanostructured metals is restricted due to their low ductility. The nanograins can not sustain a high strain hardening rate to large strains. The value of uniform elongation is only about 1-2% and then the deformation is localized, resulting in necking [2-4].

Recently, Wang et al. [5] proposed a new approach to increase the ductility of nanostructured metals. The idea is based on the development of so-called "bimodal" (composite-like) microstructures, where micrometer-size grains are embedded inside a matrix of nanocrystalline and ultra-fine grains, imparting some strain hardening capacity. In their work, pure copper was subjected to the rolling at liquid nitrogen temperature to 95% cold work [5]. The final microstructure after rolling has a grain size of 100 to 200 nm. A short annealing at 180^{o}C for 3 min resulted in a "bi-modal" grain size distribution. The majority of grains were in the nano-crystalline to ultra-fine grain range. The volume fraction of coarse grains with a grain size of 1 to 3 m was about 25%. This microstructure demonstrated an excellent combination of high strength (σ_y = 350 MPa) and uniform ductility (δ_u= 30%). Nanocrystalline grains provide high strength according to the Hall-Petch law, whereas the coarse grains improve the ductility due to their ability to accumulate dislocations during plastic deformation.

To predict the overall structure properties of composite and composite-like materials, the homogenization approaches such as the mean-field method as an analytic or semi-analytic approach and the multiscale unit cell approach as a computational method have been developed and widely applied on the basis of micromechanics. For the former, equivalent material properties are obtained through the analytical or semi-analytical solution of a boundary value problem for a spherical or ellipsoidal inclusion of one material in an infinite matrix of another material [6]. Eshelby [7] built the foundation of this method by solving the problem of the elastic field of an ellipsoidal inclusion in the surrounding matrix. In the context of the Eshelby's transformation problem, Mori and Tanaka [8] found the average stress in the matrix when the inclusion regions which have the same elastic moduli as the matrix and set up the mean-field approach for inclusions dispersed homogeneously in the matrix. On the basis of this pioneering work within the elastic range, Weng [9] developed the multiaxial theories of dual-phase plasticity in which both phases are capable of undergoing plastic flow with the applications of the Hill's decreasing constraint power of the matrix, the Berveiller-Zaoui approximation, the Mori and Tanaka's mean-field approach and the Kroner's elastic constraint.

The unit cell approach (UCA) is developed as a detailed micromechanical model with periodic boundary conditions to obtain the averaged stress-strain results for a certain prescribed deformation history and recently it has been developed as a simultaneously global-local computational procedure [10-14]. It offers the possibility of computing the macrostructural response of heterogeneous materials with an arbitrary microscopic geometry and constitutive behaviour.

However, most of previous work focuses on the materials with two-phase microstructures. The aim of this study is to study theoretically the effect of the fractal dimension on the mechanical properties of metals with multimodal

microstructure. Strictly speaking, the microstructure of copper studied in [5] is not "bi-modal", it can be described by the fractal distribution (Eq. 1) or, in other words, such materials can be referred to as materials with fractal microstructures (MFMs). For the metals with such microstructures, we develop a systematic algorithm and method including the two-step mean-field method for three-phase microstructures and the multiscale unit cell approach (UCA) using finite element modelling to predict the structure properties of such metals. As an example, pure copper with three-grain microstructures is analysed to demonstrate the validity and versatility of the proposed algorithm and method.

2. STRUCTURE PROPERTIES OF MATERIALS WITH MULTI-MODAL MICROSTRUCTURES

2.1 Volume Fraction of Multi-Modal Microstructure

Structure properties of materials with multiscale microstructures depend on the volume fraction of the "constituent phases". Considering a material with i-modal microstructures, the number of the ith-order grains with a grain size of d_i can be described by a power law relationship (fractal distribution) [15]

$$N_i = \frac{C}{d_i^D}, \tag{1}$$

where N_i is the number of grains with a grain size of d_i, C is the constant; D is the fractal dimension.

In the current study, we assume that the pure copper has a fractal microstructure containing three "phases"—the grains with the size of 100 nm, 1 m, and 10 m, respectively. The volume fraction of the grain of a given size or, in other words, the fractal dimension D, varies. In total, six different fractal microstructures with fractal dimension D = 1, 1.4, 1.8, 2.2, 2.6, and 3.0 are considered. Values of the volume fraction of the given "phases" are listed in Table 1.

Table 1. Data on the volume fraction of "phases" for a given grain size.

Fractal dimension D	1	1.4	1.8	2.2	2.6	3.0
f_1 (d=100nm)	0.9	4.8	19.6	49.3	76.1	90.1
f_2 (d=1 m)	9	19.1	31.1	31.1	19.1	9
f_3 (d=10 m)	90.1	76.1	49.3	19.6	4.8	0.9

According to the volume fraction of the grain with a given grain size listed in Table 1 and assuming the shapes of the grains are circular in two-dimensional cases, or spherical in three-dimensional cases, the numbers of the grain can be conveniently determined, which provides the geometric parameters for the design of the related finite element models.

2.2 Approximation Description of Strength and Ductility

To estimate the maximum uniform strain prior to necking in a pure metal, the well known criterion has been used [16]:

$$e = n, \tag{2}$$

where e is the maximum uniform deformation strain and n is the strain hardening coefficient [16]. For MFMs, Eq. 2 can be presented as:

$$e_{MFM} = \sum_{i=1}^{P} (e_i \cdot f_i) = \sum_{i=1}^{P} (n_i \cdot f_i) \tag{3}$$

where f_i is a volume fraction of grains of i-th order size. The volume fraction can be estimated as:

$$f_i = \frac{V_i}{V_o} = \frac{\frac{1}{6} \cdot \pi d_i^3}{V_o} \cdot N_i \tag{4}$$

Inserting Eq. 1 into Eq. 4 and the result into Eq. 3, we obtain:

$$e_{MFM} = A \cdot \sum_{i=1}^{P} \left(n_i \cdot d_i^{3-D} \right) \tag{5}$$

where, $A = \frac{\pi}{6V_o}$ and is a constant for a certain volume V_0.

Similar suggestions can be applied to strength. As known, in metals and alloys with average grain size of 100 nm and larger, strengthening with grain refinement has been rationalized on the basis of the well-known Hall-Petch mechanism [17]:

$$\sigma_y = \sigma_o + \frac{K}{\sqrt{d}} \tag{6}$$

For MFMs, Eq. 6 can be presented as:

$$\sigma_{MFM} = A \cdot \sum_{i=1}^{P} \left[\left(\sigma_o + \frac{K}{\sqrt{d_i}} \right) \cdot f_i \right] \tag{7}$$

After transformations similar to those performed for strain, Eq. 7 becomes:

$$\sigma_{MFM} = A \cdot \sum_{i=1}^{P} \left[\left(\sigma_o + \frac{K}{\sqrt{d_i}} \right) \cdot d_i^{(3-D)} \right] \qquad (8)$$

For a given material, the strain hardening coefficient n in Eq. 5 strongly depends on grain size and loading parameters. This dependence, however, demonstrates a very complicated character as different deformation mechanisms operate the plastic deformation process for the same material with different grain sizes. Thus, no clear relationship between n and d has been proposed so far. Estrin et al. [18] have proposed a phase-mixture model where numerical calculations are necessary to be performed for theoretical estimation of n. Nevertheless, the derived Eq. 5 and Eq. 8 clearly demonstrate that for a MFM, its strength and uniform ductility are determined by three parameters:

- the minimal grain size d_{min};
- the maximal grain size d_{max};
- the fractal dimension D.

The latter depends on the volume fraction of grains of each size. It can be assumed that a better combination of high strength and improved ductility can be achieved by varying these three parameters.

2.3 Mean-Field Theory for Strain-Stress Relations

The mean-field theory can be applied to estimate the stress-strain relations in pure copper with a fractal microstructure [8]. The theory was developed for two-phase metals of the inclusion matrix type where both phases are capable to undergo plastic flow. It operates on the basis of the phase averaged stress – strain fields. The average stress fields in both phases σ^1 and σ^2 are related to the global materials stress σ as [19]

$$\begin{aligned} \sigma^1 &= B^1 \sigma \\ \sigma^2 &= B^2 \sigma \end{aligned} \qquad (9)$$

Where B^1 and B^2 are stress concentration tensors. These tensors can be estimated according to Benveniste [20] as

$$\begin{aligned} B^1 &= B^1{}_{dil} \left[(1-f) I + f B^1{}_{dil} \right]^{-1} \\ B^2 &= \left[(1-f) I + f B^1{}_{dil} \right]^{-1} \end{aligned} \qquad (10)$$

where f is the volume fraction of the phase 1; I the unit tensor; and $B^1{}_{dil}$ the dilute stress concentration tensor of the phase 1. It can be estimated as [19, 20]

$$B^p{}_{dil} = \left[I + E_s^2 \left(I - S \left(E_s^{1\,-1} - E_s^{2\,-1} \right) \right)^{-1} \right] \qquad (11)$$

In Eq. (11), E^i_s is the secant moduli of the i-th phase, S the Eshelby tensor which is the function of the shape of the first phase inclusions and Poisson ratio [7]. The Poisson ratio of pure copper is $\nu = 0.33$. Young modulus $E = 71.0$ GPa.

In the present theoretical calculations, the flow stress of the i-th phases σ^i is assumed to follow the Ludwik's power-law relation

$$\sigma^i = \sigma_0^i + h^i \varepsilon^n \qquad (12)$$

where h_i is the coefficient, n is the strain hardening coefficient, and ε is the plastic strain.

2.4 Strain-Stress Relations of a Copper with Multi-modal Microstructures

True stress - strain curves of a copper with different grain size are described by the following the Ludwik's relations:

$$\begin{aligned} &\text{100 nm:} \quad \sigma = 120 + 300\varepsilon^{0.025} \quad \sigma_y = 375MPa \\ &\text{1 m:} \quad \sigma = 30 + 290\varepsilon^{0.13} \quad \sigma_y = 160MPa \\ &\text{10 m:} \quad \sigma = 40 + 280\varepsilon^{0.33} \quad \sigma_y = 75MPa \end{aligned} \qquad (13)$$

The aforementioned data on mechanical properties are taken as an approximation from [21] so that the values of yield strength for the "constituent phases" follow the Hall-Petch relationship.

In order to obtain the stress-strain relations of the pure copper with three-modal microstructures, the theoretical calculations are performed with two steps. In the first step, a two-phase microstructure with "inclusions" of a size of 1 m embedded into a matrix consisting of grains with a size of 10 m is considered. The obtained true stress-strain curve is estimated for this two-phase microstructure (Eq. 13) and it will be applied in the second step. In the second step, the pure copper is assumed as the metal with two-phase microstructure again but with the mixed structure from the first step as the matrix and "inclusions" of a grain size of 100 nm. Therefore, the true stress-strain curve for the pure copper with three-phase microstructure of 10 m, 1 m and 100nm can be determined through Eq. (13) either.

The uniform ductility ε_u is estimated according to the Considère's plastic stability criterion [16]

$$\frac{d\sigma}{d\varepsilon} = \sigma \qquad (14)$$

3. THE MULTISCALE UNIT CELL APPROACH AND FINITE ELEMENT MODELLING

3.1 The Unit Cell Approach for Metallic Materials with Multi-Modal Microstructures

Originally the unit cell approach (UCA) was developed

especially for composite structures, which contain periodically repeatable microstructures [6]. Usually the composites can be regarded as the infinite region with periodic arrangement of constituents subject to the far field mechanical loads. The most common approach for the stress and strain fields in such periodic configurations is based on describing the micro-geometry by a representative volume element (RVE) of a periodically repeating cell—the unit cell or reference cell and it has been termed as the unit cell approach (UCA). A wide variety of unit cells has been widely applied in multiscale analysis of composites in published studies.

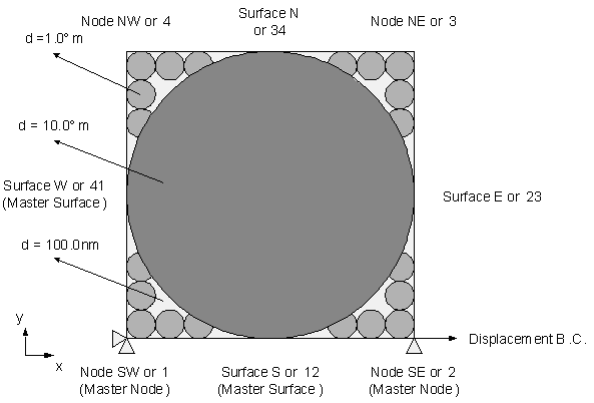

Figure 1. Three-grain unit cell model of MMC with the periodicity boundary conditions.

In the study, a three-grain unit cell model for MMC microstructures is employed in the finite element analysis for comparison as shown in Figure 1. It was devised by coupling with the periodic boundary conditions and the prescribed displacement boundary conditions to obtain the macroscopic material elastoplastic properties through averaging the stress and strain obtained in micro level.

The related periodic boundary conditions can be described and defined through two master surfaces, S and W and two master nodes, SW and SE, according to Figure 1:

$$\begin{aligned} u_N - u_S &= u_{NW};\ v_N - v_S = v_{NW} \\ u_E - u_W &= u_{SE};\ v_E - v_W = v_{SE} \\ u_{NE} - u_{NW} &= u_{SE};\ v_{NE} - v_{NW} = v_{SE} \end{aligned} \tag{15}$$

where, u and v is the components of the displacement tensor in x and y directions for two-dimensional problems, respectively. To constrain the rigid-body motions, the degrees of freedom at master nodes, SW and SE, are also fixed as follows:

$$u_{SW} = 0,\ v_{SW} = 0 \text{ and } v_{SE} = 0 \tag{16}$$

The prescribed displacement boundary condition is only applied at the x-direction in the master node SE for the displacement driven unit cell approach.

3.2 Multi-scale Modeling from Micro to Macro-Localization and Homogenization

In the typical periodic micro-field approach, stresses and strains are split into two parts: constant macroscopic contributions—slow variables, $\langle\varepsilon\rangle$ and $\langle\sigma\rangle$; and periodically varying microscopic fluctuation—fast variables, $\langle\varepsilon'(\mathbf{x})\rangle$ and $\langle\sigma'(\mathbf{x})\rangle$, where $\mathbf{x}$ is the position vector of 2-D unit cell, $\mathbf{x} = x_1\mathbf{e}_1 + x_2\mathbf{e}_2$, and x_1 and x_2 are related to a fixed rectangular Cartesian coordinate system, $\boldsymbol{e}_1$ and $\boldsymbol{e}_2$ are two components of unit base vectors of the coordinate system. The volume averages of the latter vanish for sufficiently large integration volumes,

$$\frac{1}{V_U}\int_{V_U}\sigma'(\mathbf{x})dV_U = \frac{1}{V_U}\int_{V_U}\varepsilon'(\mathbf{x})dV_U = 0 \tag{17}$$

If the region is sufficiently large with no significant macroscopic gradients of stress, strain or composition, macroscopic stresses and strains can be obtained through the homogenization and localization method by volume averages,

$$\begin{aligned} \langle\sigma\rangle &= \frac{1}{\Omega_U}\int_{\Omega_U}\sigma(\mathbf{z})d\Omega \\ &= \frac{1}{2\Omega_U}\int_{\Gamma_U}\left[\mathbf{u}(\mathbf{z})\otimes\mathbf{n}_\Gamma + \mathbf{n}_\Gamma\otimes\mathbf{u}(\mathbf{z})\right]\sigma(\mathbf{z})d\Gamma \end{aligned} \tag{18}$$

$$\begin{aligned} \langle\varepsilon\rangle &= \frac{1}{\Omega_U}\int_{\Omega_U}\varepsilon(\mathbf{z})d\Omega \\ &= \frac{1}{2\Omega_U}\int_{\Gamma_U}\left[\mathbf{t}(\mathbf{z})\otimes\mathbf{z}\right]d\Gamma \end{aligned} \tag{19}$$

where, $\langle\bullet\rangle$ stands for volume average, σ and ε are stress and strain tensors (vectors in Voigt notation), respectively. Ω_U and Γ_U stand for the volume and the surface of the unit cell model of the different configurations including the reference or initial configuration and current or deformed configuration.

Macroscopic measurements can be obtained as a volume average of their microscopic counterparts. The remaining macroscopic measures are then expressed in terms of these average quantities using the classic continuum mechanics relations. For finite deformation, the deformation gradient, $\mathbf{F_m}$, the first Piola-Kirchhoff stress tensor $\mathbf{P_m}$ and their rates are suitable for the purpose of averaging.

For a unit cell model with the prescribed displacement boundary conditions, the position vector of a point in the boundaries of the unit cell model in the deformed or current state is given as

$$\mathbf{x} = \mathbf{F}_m \cdot \mathbf{X} \tag{20}$$

where, $\mathbf{X}$ is the position vector of the point in the undeformed boundary Γ_0.
The traction boundary conditions can be prescribed as

$$\mathbf{t} = \mathbf{n_0} \cdot \boldsymbol{\sigma}_m \qquad \text{on } \Gamma \tag{21}$$

or

$$\mathbf{p} = \mathbf{n_t} \cdot \mathbf{P}_m^T \qquad \text{on } \Gamma_0 \tag{22}$$

The macroscopic deformation gradient tensor $\mathbf{F}_M$ and the macroscopic first Piola-Kirchhoff stress tensor $\mathbf{P}_M$ are the volume average of the microscopic gradient tensor $\mathbf{F}_m$ and the microscopic first Piola-Kirchhoff stress tensor $\mathbf{P}_m$, respectively,

$$\mathbf{F}_M = \frac{1}{V_0}\int_{V_0} \mathbf{F}_m dV_0 \tag{23}$$

$$\mathbf{P}_M = \frac{1}{V_0}\int_{V_0} \mathbf{P}_m dV_0 \tag{24}$$

According to the divergence theorem, the abovementioned volume integrals can be transformed into surface integrals over the outward surface of the unit cell model, resulting in

$$\mathbf{F}_M = \frac{1}{V_0}\int_{\Gamma_0} \mathbf{x}\mathbf{n}_0 d\Gamma_0 \tag{25}$$

$$\mathbf{P}_M = \frac{1}{V_0}\int_{\Gamma_0} \mathbf{p}\mathbf{X} d\Gamma_0 \tag{26}$$

For the case of a two-dimensional unit cell model with prescribed displacement boundary conditions, they can be further simplified as

$$\mathbf{F}_M = \frac{1}{V_0}\sum_{i=1}^{n_\Gamma} \mathbf{x}_i \mathbf{n}_{0i} l_i \tag{27}$$

$$\mathbf{P}_M = \frac{1}{V_0}\sum_{i=1}^{n_\Gamma} \mathbf{p}_i \mathbf{X}_i l_i \tag{28}$$

where n_Γ is the total number of nodes along the boundary Γ and l_i is the side length between two neighboring nodes i and $i+1$ or $i-1$ and i in the initial configuration.

Further for the present 2-D displacement-driven square unit cell model, considering the periodicity boundary conditions and

$$\mathbf{F}_M = \frac{1}{V_0}\left[\left(\mathbf{x}_4 - \mathbf{x}_1\right)\mathbf{n}_{43}^0 \left\|\mathbf{x}_2^0 - \mathbf{x}_1^0\right\| + \left(\mathbf{x}_2 - \mathbf{x}_1\right)\mathbf{n}_{23}^0 \left\|\mathbf{x}_4^0 - \mathbf{x}_1^0\right\| \right] \tag{29}$$

Also, through the force equilibrium on the resultant external forces in the nodes along the outward surface caused by $\mathbf{P}_M$ and the reaction forces in the four corner points

$$\mathbf{P}_M = \frac{1}{V_0}\sum_{i=1}^{n_C} \mathbf{f}_i \otimes \mathbf{X}_i \tag{30}$$

where, $\otimes$ stands for dyadic product of two vectors, $\boldsymbol{f}_i$ is the external reaction forces at the corner points in the square unit cell model and i = 1 and 2 for the present boundary conditions. Note that $\mathbf{P}_M$ is an unsymmetrical 2nd-order tensor for 2-D cases.

Therefore, the macroscopy-microscopy transformation of the deformation gradient $\mathbf{F}$ and the first Piola-Kirchhoff stress tensor $\mathbf{P}$ can be obtained easily through the data outputs of the coordinates, displacements and reaction forces at these two corner points from the present unit cell model.

Furthermore, according to the classic continuum mechanics, the macroscopic Green-Lagrange (True) strain and Cauchy (True) stress tensor can be obtained, respectively,

$$\boldsymbol{\varepsilon}_M = \frac{1}{2}\left(\mathbf{F}_M^T \cdot \mathbf{F}_M - \mathbf{I}\right) \tag{31}$$

$$\boldsymbol{\sigma}_M = \frac{1}{J}\mathbf{P}_M \cdot \mathbf{F}_M^T \tag{32}$$

where, $J = \det\left(\mathbf{F}_M\right) = \dfrac{V}{V_0}$.

3.3 Finite Element Modeling of the Unit Cell

Two-dimensional FE models for the plane strain problem are devised in this work. In the 2-D FE models, the grains with different sizes are simulated using different parts defined by the related material properties, which follow the abovementioned Ludwik's stress-strain relations defined in Eq. (13). The grains of different size were assumed to be bonded to each other perfectly and thus the contact problems between these grains are neglected. Further, to simplify the modelling process, only the grains with sizes of 10.0 m and 1.0 m are created and the rest domains are assumed to be fully occupied by the smallest grains of 100.0 nm as the third phase. The shapes of the grains of 10.0 m and 1.0 m were designed as circular only.

Three models are designed for the cases with the fractal dimension as 1.4, 1.8 and 2.2 and they have different cell sizes. For the case of fractal dimension D = 1.4, the 2-D unit cell FE model is devised with a square control domain of 10.0 m×10.0 m and they are discretized using the refined meshing by the mixing usage of

quadrilateral and triangular plane strain elements. The quadrilateral elements were used to discretize the circular particles with the grain sizes of 10.0 m and 1.0 m and the triangular elements occupied the remaining regions due to their geometric complexity. For the cases of fractal dimension D = 1.8 and 2.2, the size of the unit cell model was designed as 20.0 m×20.0 m for catching the periodically repeating microstructures.

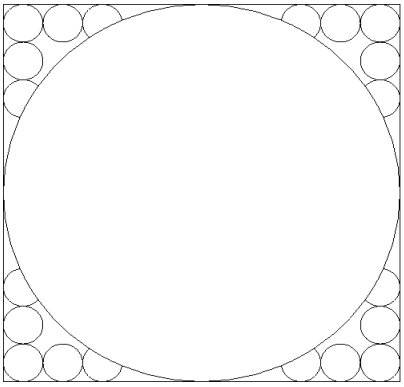

(a) Fractal dimension D = 1.4

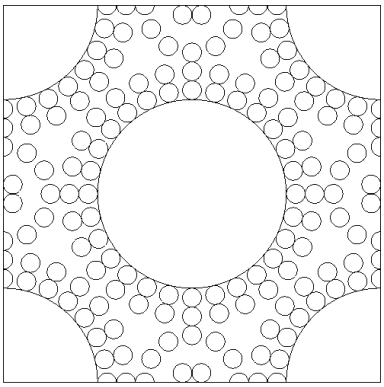

(b) Fractal dimension D = 1.8

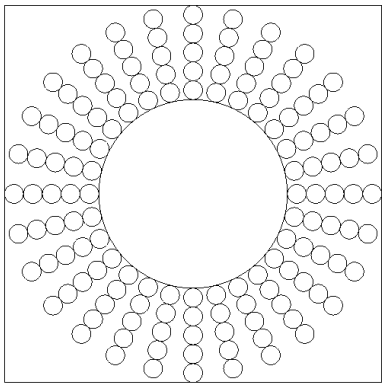

(c) Fractal dimension D = 2.2

Figure 2. Geometric configurations of the unit cell models of pure copper with three-grain microstructures at fractal dimensions of 1.4, 1.8 and 2.2.

The related meshes were still constructed by mixing the quadrilateral and triangular plane strain elements. Note that to simplify the modelling procedure, all the unit cell models were designed in the symmetrically-distributed manner of the grains of 10.0 m and 1.0 m, without considering the influence from their different spatial distribution. The typical finite element mesh for D = 1.4 is shown in Figure 3. The FE meshes were created using ABAQUS/CAE and note that the periodicity boundary conditions are prescribed using the MPC-constrain option by linear equations according to Eqs. (15) and (16).

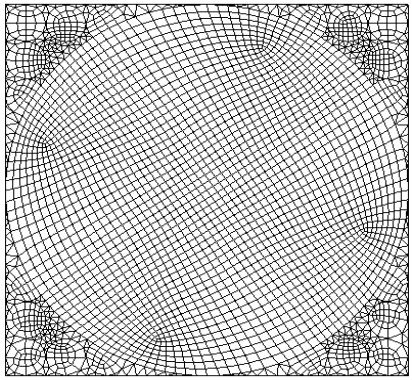

Figure 3. Typical mesh of three-phase unit cell model for D = 1.4.

The loading cases for different stress/strain levels in MMC were simulated and performed by applying the prescribed displacement boundary condition in the master node, SE or 2, in x direction from 5.0e-6mm to 5.0e-3 mm for D = 1.4 and from 1.0e-5mm to 10.0e-3mm for D = 1.8 and 2.2, which leads to the related true strain of exceeding 0.5 in macro level.

4. RESULTS AND DISCUSSION

4.1 Theoretical Solutions

The true stress – strain curves for pure copper with different grain sizes are plotted according to Eq. 13 and the pure copper with fractal microstructure $D = 2.2$ obtain from the proposed two-step mean-field method is also demonstrated in Figure 4 for comparisons. It is reasonable the flow curve of the pure copper with fractal microstructure $D = 2.2$ is much higher than those of the pure copper with single phase of 1.0 m and 100.0nm but lower than the one with single phase of 10.0 m.

The results of theoretical calculations including the yield strength σ_y, the ultimate tensile strength σ_{UTS} and the uniform strain ε_u of the pure copper with three-grain microstructure are listed in Table 2. The yield strength σ_y and the ultimate tensile strength σ_{UTS} of the pure copper with three-grain microstructure gradually increase with increasing fractal dimension D from 1.0 to 3.0 whereas the uniform strain ε_u estimated by the Considere's criterion decreases.

Table 2 Theoretical results on mechanical properties of the pure copper with fractal microstructure.

D	σ_y MPa	σ_1 MPa	σ_{UTS} MPa	ε_u %
1	82	109	223	24.4
1.4	89	120	229	21.8
1.8	121	164	254	13.9
2.2	185	253	302	6.9
2.6	280	336	351	3.6
3.0	350	368	375	2.5

However, this dependence does not coincide completely to the experimental results reported in [5], which are depicted in Figure 5, comparing the results depicted in Figure 6. In fact, none of the fractal microstructures demonstrates such a high combination of high strength and ductility as in [5]. Representative tensile curves theoretically estimated for the pure copper with fractal microstructure (Figure 4) are similar to those for the conventional, ultra-fine and nano-crystalline pure copper (Figure 5).

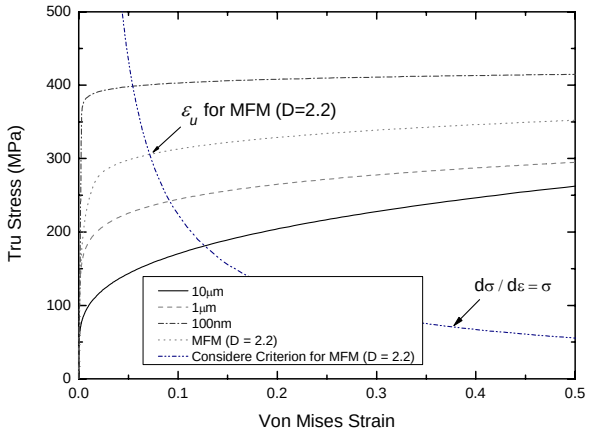

Figure 4. True stress – strain curves for pure copper with different microstructures: d = 100 nm, 1 m, 10 m, and fractal microstructure with D = 2.2.

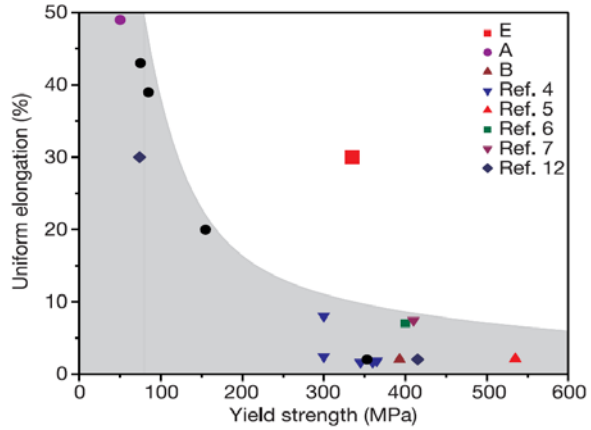

Figure 5. Representative tensile curves for pure copper with fractal microstructure (different fractal dimensions) [5].

There are a few reasons to explain such a behaviour. It has been reported that nanostructured metals demonstrate strain-rate sensitivity even at room temperature [21-23]. For pure copper, the strain rate sensitivity increases with decreasing grain size and is about of $m = 0.03$ for $d = 100$ nm [21-23]. The increased strain rate sensitivity delays necking, thereby improving uniform elongation [17]. Hart's criterion has been used to predict the uniform elongation of strain rate sensitive nanomaterials [16]

$$\frac{d\sigma}{\sigma d\varepsilon} + m = 1 \qquad (15)$$

This criterion, however, cannot be applied in our case as:

1) The values of the strain rate sensitivity for bimodal materials or materials with multimodal microstructures have not been reported so far;
2) Plastic deformation is inhomogeneous within the material in materials with bi- or multi-modal microstructures. It is localized within coarse grains and spreads within materials. Therefore, local values of the deformation strain rate are also inhomogeneous within the material. The local values of the deformation strain rate are higher for coarse grains and significantly smaller in the area of ultra-fine and nanograins, as the deformation is localized within the coarse grains.

The latter effect might increase the uniform elongation of both the local areas of the ultra-fine and nanograins and the bi-modal (or MFM) as the coarse-grained microstructures are not strain-rate sensitive and demonstrate high values of uniform elongation.

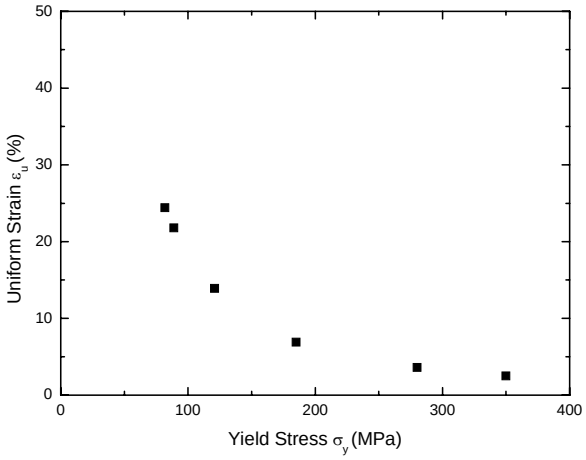

Figure 6. Representative tensile curves for pure copper with fractal microstructure.

4.2 Numerical Results from the Unit Cell Approach

Numerical simulations were performed using ABAQUS/Standard Version 6.6-4 and the deformation

and Von Mises Stress contours of the FE models of fractal dimension D = 1.4, 1.8 and 2.2 subject to the prescribed displacement along x direction at the master node SE are shown in Figure 7. Note that the different magnitude of the displacement was applied to ensure the same strain levels obtained for the unit cell models of different unit cell.

The post-processing of the average stress and strain tensors from the unit cell models using FEA is processed using a self-developed FORTRAN program, which can collect the reaction forces and displacements as well as the related node coordinates at the corners nodes in the unit cell models from the related input and output files. The true stress and strain curves at the macro level can be thus generated by taking an overall average through the whole control volume of the unit cell model according to Eqs. (31) and (32).

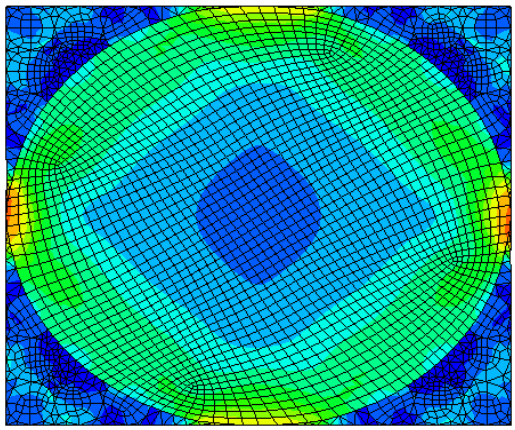

(a) D = 1.4, x = 0.001 mm

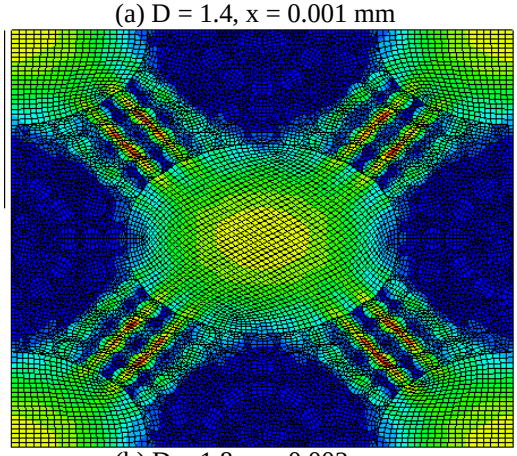

(b) D = 1.8, x = 0.002 mm

Figure 7. Von Misses stress contours in the deformed domain of unit cell models (D = 1.4, 1.8) subject to the prescribed displacement boundary condition at master node SE.

The extracted results as relations of the macroscopic true stress σ and strain ε for all the three cases with fractal dimension D = 1.4, 1.8 and 2.2 are plotted in Figure 8. As shown in Figure 8, the true stress of the pure copper with the three-grain microstructure gradually increase with increasing fractal dimension D from 1.4 to 2.2, which is similar to those results from the proposed two-step mean-field method.

For comparison, the theoretical solutions for D = 2.2 is also plotted in Figure 8 and the numerical results from the multiscale unit cell approach for the same D have a reasonable agreement with them. The differences between the two groups of data may be caused by spatial effects ignored in the unit cell approach and mean-field method. The former depends on the spatial distribution, shapes of the grains of different grain whereas the latter is generic without consideration of the spatial distributions of the grains, only with the homogenous distribution instead. Moreover, the derivation may be also from the designed microstructure which the unit cell models applied in the current analysis are all involved in the cases only containing a central-located grain with the biggest grain size, referring to Figs. 2 and 7.

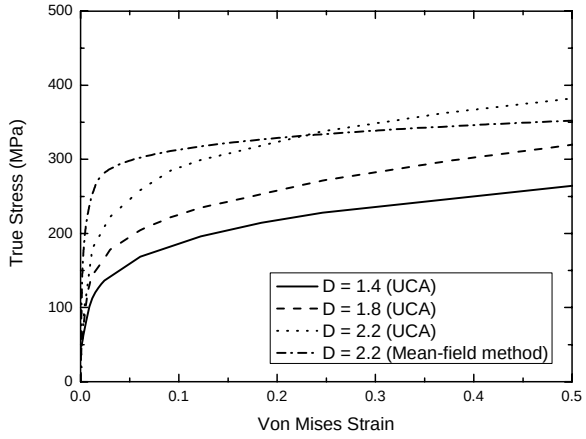

Figure 8. The true stress-strain relations of pure copper with three-grain microstructures at fractal dimension D = 1.4, 1.8 and 2.2.

5. CONCLUSION AND FUTURE WORK

To investigate the structure-property relations of the metals with multiscale (three-grain) microstructures, a modified theoretical approach—two-step mean-field method and a computational method—the multiscale unit cell approach were both developed and applied in the current study. The results of pure copper with three-grain microstructures from these two proposed approaches had a reasonable agreement and the differences between them were caused by the natures of them. One of the advantages of the proposed FEM-based multiscale unit cell approach over the modified mean-field method for multiscale microstructure is that it can flexibly handle the complex geometry of the microstructures including spatial distribution, shapes of grains.

The present theoretical analysis algorithm and computational strategy is being extended to study the following 2-D problems. On the one hand, for ideal microstructures using unit cell methods, size effect and optimal size of unit cell model for metal matrix composites (MMC), spatial effects of the grains with different sizes on material mechanical properties and shape effects of grains with different geometries such as circular, elliptic and line-like; and extensive analyses

about the multiscale unit cell models including the influences from applied boundary conditions, applications of dummy nodes and the different average methods of stress and strain. On the other hand, for real and quasi-real microstructures using unit cell methods, numerical simulations of the real and quasi-real MMC microstructures according to digital images from SEM can be performed by the proposed multiscale unit cell approach conveniently. Furthermore, the study will be also performed extensively from 2-D problems to 3-D problems, even for the microstructures containing damage or defect in the future with the considerations of damage growth and propagation.

Acknowledgement

The authors would like to appreciate the financial supports from Australian Research Council (ARC) through Prof. Peter Hodgson's Federation Fellowship (FF0455846).

References

1. M.A. Meyers, A. Mishra, D.J. Benson, *Prog Mater Sci*, 2006, vol. 51, pp. 427-556.
2. P.G. Sanders, J.A. Eastman, J.R. Weertman. *Acta Mater*, 1997, vol.45, pp. 4019–4025.
3. M. Lergos, B.R. Elliott, M.N. Rittner, J.R. Weertman, K.J. Hemker. *Phil. Mag*, 2000, vol. A80, pp. 1017–1026.
4. R.Z. Valiev, I.V. Alexandrov, Y.T. Zhu, T.C. Lowe. *J. Mater. Res*, 2002, vol. 17, pp. 5–8.
5. Y. Wang, M. Chen, F. Zhou, E. Ma. *Nature*, 2002, vol. 419, pp. 912-915.
6. S. Nemat-Nasser and M. Hori, Micromechanics: overall properties of heterogeneous materials, Elsevier science publisher, Netherlands, 1993.
7. J.D. Eshelby. *Proc. R. Soc. Lond*, 1957, vol. A241, pp. 376-386.
8. T. Mori, K. Tanaka. *Acta Metall*, 1973, vol. 21, pp. 571-583.
9. G. J.Weng, J.Mech. Phys. Solid, I990, Vol. 38, No. 3, pp. 419–441.
10. Smit, R. J. M., Brekelmans, W. A. M., and Meijer, H. E. H. *Comput. Methods Appl. Mech. Engrg.*, 1998, Vol. 155, pp.181–192.
11. Smit, R. J. M., Brekelmans, W. A. M., and Meijer, H. E. H. *J. Mech. Phys. Solids*, 1999, Vol. 47, pp. 201–221.
12. Kouznetsova, V., Brekelmans, W. A. M., and Baaijens, F. P. T., *Comput. Mech.*, 2001. Vol. 27, pp.37–48.
13. Terada, K., Hori, M., Kyoya, T., and Kikuchi, N, Int. J. Solids Structures, .2000, Vol. 37, pp.2285–2311.
14. Terada, K. and Kikuchi, N., Comput. Methods Appl. Mech. Engrg., 2001, Vol. 190, pp.5427–5464.
15. Mandelbrodt BB. The fractal geometry of nature. New-York, USA, Freeman, 1982.
16. G.F. Dieter, Mechanical metallurgy (3rd ed.), McGraw Hill, New York, 1986.
17. K.S. Kumar, H. Van Swygenhoven, S. Suresh. *Acta Mater*, 2003, vol. 51, pp. 5743-5774.
18. H.S. Kim, Y. Estrin, *Acta Mater*, 2005, vol. 53, pp. 765-772.
19. R.J. Hill, *J. Mech. Phys. Solids*, 1965, vol. 13, pp. 89-99.
20. Y. Benveniste, *Mech. Mater*, 1987, vol. 6, pp. 147-159.
21. K.C. Siow, A.A.O. Tay, P. Oruganti. *Mater Sci Tech*, 2004, vol. 20, pp. 285-294.
22. M. Dao, L. Lu, Y.F. Shen, S. Suresh, *Acta Mater*, 2006, vol. 54, pp. 5421-5432.
23. R. Schwaiger, B. Moser, M. Dao, N. Chollacoop, S. Suresh, *Acta Mater*, 2003, vol. 51, pp. 5159-5172.
24. Hibbitt, Karlsson and Sorensen Inc., ABAQUS user's manual V6.6, 2006.